NASA Technical Memorandum 105394

Creep and Stress Relaxation Modeling of Polycrystalline Ceramic Fibers

James A. DiCarlo
Lewis Research Center
Cleveland, Ohio

and

Gregory N. Morscher
Case Western Reserve University
Cleveland, Ohio

Prepared for the
1991 Winter Annual Meeting
sponsored by the American Society of Mechanical Engineers
Atlanta, Georgia, December 1–6, 1991

National Aeronautics and
Space Administration

CREEP AND STRESS RELAXATION MODELING OF POLYCRYSTALLINE CERAMIC FIBERS

James A. DiCarlo
National Aeronautics and Space Administration
Lewis Research Center
Cleveland, Ohio 44135

and

Gregory N. Morscher*
Case Western Reserve University
Cleveland, Ohio 44106

E-6785

SUMMARY

A variety of high performance polycrystalline ceramic fibers are currently being considered as reinforcement for high temperature ceramic matrix composites. However, under mechanical loading above 800 °C, these fibers display creep-related instabilities which can result in detrimental changes in composite dimensions, strength, and internal stress distributions. As a first step toward understanding these effects, this study examines the validity of a mechanism-based empirical model which describes primary stage tensile creep and stress relaxation of polycrystalline ceramic fibers as independent functions of time, temperature, and applied stress or strain. To verify these functional dependencies, a simple bend test is used to measure stress relaxation for four types of commercial ceramic fibers for which direct tensile creep data are available. These fibers include both nonoxide (SCS-6, Nicalon) and oxide (PRD-166, FP) compositions. The results of the bend stress relaxation (BSR) test not only confirm the stress, time, and temperature dependencies predicted by the model, but also allow measurement of model empirical parameters for the four fiber types. In addition, comparison of model tensile creep predictions based on the BSR test results with the literature data show good agreement, supporting both the predictive capability of the model and the use of the BSR test as a simple method for parameter determination for other fibers.

NOMENCLATURE

A_o	empirical creep strain parameter
B	empirical thermal parameter, K^{-1}
E	elastic modulus, GPa
J_c	creep compliance, GPa^{-1}
Q	creep activation energy, kJ/mol
R	gas constant, 8.314 J/mol-K
R_a	final fiber loop radius after stress relaxation, mm

*NASA Resident Research Associate at Lewis Research Center.

R_o	initial fiber loop radius, mm
T	test temperature, K
d	fiber diameter, μm
m	bend stress relaxation (BSR) ratio
m′	tensile stress relaxation ratio
n	empirical stress exponent
p	empirical time exponent
t	test time, s, hr
$\Delta(1/T)$	change in reciprocal temperature at constant m or ε_c for one decade time change, K^{-1}
ε_c	tensile creep strain
ε_e	tensile elastic strain
$\varepsilon_c/\varepsilon_e$	normalized tensile creep strain
ε_o	applied surface strain
γ	time-temperature variable
γ_o	time-temperature constant
σ	applied local stress, GPa
σ'	average applied tensile stress, GPa
τ	relaxation time, s
τ_o	relaxation time at infinite temperature, s

INTRODUCTION

For a structural composite, it is desirable that the reinforcing fibers display high stiffness (modulus) and high strength relative to the matrix, and maintain these properties to as high a temperature as possible. Among other benefits, this allows the composite to operate in the elastic range to high stresses over a wide temperature range. For polymer and metal matrix composites reinforced by currently available ceramic fibers, this condition is generally achieved up to the maximum use temperatures of these composites. This is the case because use-limiting effects are typically related to the matrix (e.g., oxidation, plasticity) and occur at temperatures lower than ~800 °C where current ceramic fibers first begin to show significant creep-related stiffness and strength degradation (DiCarlo, 1991). For ceramic matrix composites (CMC), however, this loss in fiber structural properties can occur in the use temperature

ranges projected for a variety of high performance structural applications. Indeed, in some cases, current ceramic fibers show stiffness and strength losses at temperatures well below those where similar effects occur in potential ceramic matrices. At the present time, the structural implications for these effects have not been fully comprehended, either experimentally or theoretically. Clearly, critical questions arise as to whether for any CMC application above 800 °C, the creep-related change in dimensions and associated loss in structural properties displayed by current ceramic fibers can be tolerated and, if not, what minimum properties should be displayed by the reinforcing fiber.

The objective of the present study is to take a first step toward answering these questions. Because CMC fail brittlely at strains much less than one percent, this work addresses the issue of modeling and measuring the initial stages of creep and stress relaxation of polycrystalline ceramic fiber reinforcement. To accomplish this, an empirical model is proposed which has been found to phenomenologically describe primary stage tensile creep of SiC polycrystalline fibers as a function of stress, time, and temperature. This model is then further expanded to include a description of fiber stress relaxation. To determine the general applicability of the model, stress relaxation is then measured on four types of commercial fibers for which tensile creep data exist in the literature. These measurements are made by the recently developed bend stress relaxation (BSR) test which for fibers is much more convenient, but less direct, than a typical tensile creep test (Morscher and DiCarlo, 1991). In each case, good functional and quantitative agreement is shown between the model predictions and available tensile creep data, thereby supporting general use of the model and the simple BSR test to estimate creep and stress relaxation of current and future polycrystalline fibers.

APPROACH

Tensile Creep Model

In order to fully understand the effects of ceramic fiber creep on CMC structural performance, it is important to develop a model which describes total creep strain for the fibers of interest. Because the majority of ceramic fibers are polycrystalline in nature and because many of these fibers display a relatively large creep deformation in the primary stage, an empirical model is proposed here which has been found to describe fairly well the total tensile creep strain that occurs in the primary creep stage of chemically vapor-deposited (CVD) polycrystalline SiC fibers. As will be discussed, this model can be related to microstructural phenomena and thus is considered more advanced than traditional primary stage empirical models (Andrade, 1910; Feltham, 1953).

Under constant tensile stress and constant temperature from 1000 to 1400 °C, CVD SiC fibers creep in the primary or transient stage with no evidence of steady state creep for strains up to at least 0.3 percent (DiCarlo, 1986). For these conditions, creep deformation can be described fairly accurately by linear anelastic theory (Nowick and Berry, 1982); that is,

$$\varepsilon_c = \sigma J_c(\gamma) \tag{1}$$

where ε_c is total tensile creep strain, σ is the applied stress, and J_c is the fiber creep compliance which is dependent on the time-temperature variable γ given by

$$\gamma = \ln t - Q/RT. \tag{2}$$

Here t and T are the test time (s) and test temperature (K), respectively; R is the gas constant, 8.314 J/mol-K; and Q is the controlling creep energy. The compliance J_c is effectively zero for $\gamma < \gamma_o$, but grows exponentially with γ for $\gamma > \gamma_o$. This behavior allows J_c to be described empirically by the simple relation

$$J_c(\gamma) = J_c(\gamma_o)\exp[p(\gamma - \gamma_o)] \tag{3}$$

where $J_c(\gamma_o)$ and p are experimentally determined parameters. For example, for as-received CVD SiC fibers, perceptible creep begins above $\gamma_o \approx -35$, yielding $J_c(\gamma_o) \approx 10^{-3}$ $(GPa)^{-1}$ and $p \approx 0.36$ (DiCarlo, 1986). Heat treatment of the fibers prior to creep testing was observed to reduce p with increasing treatment temperature.

The creep behavior described above for CVD SiC fibers is very similar to that observed for polycrystalline aluminum wires in the classic creep studies of Ke and Zener (1947, 1950). For this reason, it appears that much of the underlying phenomena can be explained in the same way for both materials. That is, fiber creep in the primary stage is the result of thermally-activated grain boundary sliding or relaxation which is controlled by atomic diffusion at the grain boundary. The microscopic sliding of each grain-related entity can thus be characterized by a relaxation time τ given by

$$\tau = \tau_o \exp(Q/RT) \tag{4}$$

where τ_o is the relaxation time at infinite T and Q is the controlling activation energy. For the aluminum wires and SiC fibers, all creep entities for each system appear to have the same energy Q, but are broadly distributed in τ_o beginning above the relaxation time $\tau_o \approx 10^{-15}$. Assuming each entity slides or relaxes when $t = \tau$ and defining $\gamma = \ln(\tau_o)$, the phenomenological bases for equation (2) and $\gamma_o \approx -35$ can be understood. In addition, it would appear that the parameter p in equation (3) is structure sensitive. Finally, the explanation for the exponential rise in creep with $\gamma = \ln(\tau_o)$ is not clear. Ke and Zener (1950) as well as Feltham (1955) offer models which assume that τ_o increases with the size of the creep entities. This suggests that as time increases, equation (3) creep is the result of the relaxation of larger and larger groups of grains which contribute an exponentially increasing creep strain.

In this study, it is assumed that the creep compliance of all polycrystalline fibers in the primary stage can be described by equation (3). Support for this assumption can be developed by using equation (2) to obtain a direct dependence of J_c on time and temperature. For example, simple manipulation of these equations yields

$$J_c(t,T) = J_c(\gamma_o)[t^p][\exp(-pQ/RT)]\ [\exp(-p\gamma_o)]. \tag{5}$$

At constant temperature, it can be seen that J_c increases with t^p and since $p \approx 1/3$, equation (5) effectively becomes Andrade's classic creep equation which has been observed to describe primary or transient stage creep for a variety of polycrystalline materials (Andrade, 1910). However, creep equations (3) and (5) are more general than Andrade's law in that they allow time and temperature to be combined into a single variable γ and also allow the parameter p to vary with structure changes that can occur, for example, as a result of heat treatment. In addition, the equation (5) model predicts that creep and creep rate in the primary stage are not directly controlled by the activation energy Q but by an effective energy pQ. This is an important point which could be the source of the apparently low

energy values measured in some studies which assume steady state conditions for the low temperature creep of Si-based fibers (Tressler and Pysher, 1990) and monoliths (Sargent and Ashby, 1983).

Although many polycrystalline ceramics will display the linear stress dependence assumed in equation (1), it will be shown that, during the primary stage, the commercial fibers tested in this study creep with a stress power dependence σ^n with the empirical parameter n slightly greater than unity, i.e., $1 \leq n < 2$. To account for these observations (whose underlying mechanisms are currently unclear), a more general model is proposed; i.e.,

$$\varepsilon_c = \sigma J_c(\sigma,\gamma). \tag{6}$$

Here J_c is allowed to maintain its definition as a creep compliance, but absorbs the additional stress dependence above $n = 1$. Equation (6) can be further simplified by introducing the parameters

$$A(\sigma,p) = J_c(\sigma,\gamma_o)\exp[-p\gamma_o] = A_o(p,\gamma_o)\sigma^{n-1} \tag{7a}$$

and

$$B(p) = pQ/R, \tag{7b}$$

so that by equations (5) to (7),

$$\varepsilon_c = A_o\, \sigma^n\, t^p\, \exp[-B/T]. \tag{8}$$

Equation (8) represents the general model proposed here for primary stage tensile creep of polycrystalline ceramic fibers. Clearly it assumes that under constant stress and temperature conditions, primary stage creep strain displays simple power dependences on stress and time and an exponential dependence on reciprocal temperature. The objective of the remaining portion of this study is to determine whether this mechanistic-based model adequately describes the creep behavior of selected polycrystalline ceramic fibers.

Bend Stress Relaxation Test

Although direct tensile testing under constant stress and temperature is the preferred method to verify the equation (8) creep model, there are many experimental problems with this approach. These center primarily on the difficulties associated with accurately measuring the displacement of two points on a long, fragile, small diameter fiber that must be held at a constant temperature between points. Typically this will require furnaces with long uniform hot zones, mechanical grips which can be heated to the fiber temperature with little chemical reaction with the fiber, controlled test environments to avoid fiber environmental degradation, and remote sensors to avoid mechanical loading artifacts. In addition, there is need to correct for elastic deformation and conduct many experimental runs to establish time, temperature, and stress dependencies and to determine statistical variations. This can be a special concern for some newly developed fibers which are not available in large quantities nor in long lengths. It is probably issues such as these which underlay the fact that very little tensile creep data presently exist in the literature for fibers of current technical interest.

To circumvent some of the inconveniences of the tensile test, the approach in this study is to utilize the bend stress relaxation (BSR) test which is described in greater detail elsewhere (Morscher and DiCarlo, 1991). For this test, a short length of fiber is held at constant strain in a pure bending mode

while being thermally treated for a specific time at constant temperature in a controlled environment. For small diameter fibers, bending modes of different applied strains can be achieved by tying the fibers into small loops of different radii R_o. After treatment, the fiber loops are broken at room temperature, leaving creep-induced curves in the fiber of radii R_a. For a test time t at temperature T, it is convenient to define a bend ratio m given by

$$m(\varepsilon_o,t,T) = 1 - R_o/R_a \tag{9}$$

where $\varepsilon_o = d/2R_o$ is the maximum applied bend strain on the surface of a fiber of diameter d. The ratio m is a quantitative measure of creep effects in the fiber, ranging in value from unity for elastic behavior ($R_a = \infty$) to zero for total stress relaxation ($R_a = R_o$).

For fibers of uniform isotropic microstructure and creep behavior linear with stress (n = 1), the ratio m given by equation (9) is independent of ε_o and thus is an accurate measure of the relative amount of creep-induced stress relaxation that occurs at each position in the fiber; i.e.,

$$m = \sigma(t,T)/\sigma(0,T) = m'. \tag{10}$$

As indicated, the m ratio measured in pure bending is also exactly equivalent to m′, the stress relaxation ratio that one would measure for these fibers under pure tensile loading for any applied strain. However, for nonuniform fibers or uniform fibers with n > 1, the bend m ratio represents a weighted average of local stress relaxations in the fiber. For the case of nonuniform fibers, the m ratio could be larger or smaller than the tensile m′ ratio, depending on the nature, location, and orientation of the creeping phases within the fiber. For the case of uniform fibers with n > 1, the bend m ratio will depend on the applied surface strain ε_o. Because the outer layers of the fibers in bend will stress relax more than the inner layers, the bend m ratio measured at ε_o will be greater than the tensile m′ ratio measured at the same but uniform ε_o.

For model verification in the primary stage, it follows then that the BSR test has both advantages and disadvantages in comparison to the direct tensile test. Advantages described in more detail elsewhere (Morscher and DiCarlo, 1991) include the ability to eliminate grips, sensors, and the need for long continuous fibers and test chambers; the ability to avoid the elastic strain correction and to study many specimens at the same time under controlled environmental and pressure conditions; and, for certain fibers, the ability to accurately measure the stress relaxation ratio m′ that will occur in a fiber under pure tensile loading. Disadvantages center primarily on the inability to yield continuous real-time measurements and the fact that the m ratio measured in bending is not always an accurate measure of the stress relaxation ratio m′.

Under certain conditions, however, m bend data can be equated to m′ tensile data which in turn can be converted directly into tensile creep strain by the simple relation

$$\varepsilon_c/\varepsilon_e = \varepsilon_c E/\sigma = (1/m') - 1 = (1/m) - 1. \tag{11}$$

Here E is fiber elastic modulus, $\varepsilon_e = \sigma/E$ is tensile elastic strain, and $\varepsilon_c/\varepsilon_e$ is defined as the normalized tensile creep strain ratio. As discussed earlier, the conditions for the m = m′ equality are fibers with linear stress dependences and uniform isotropic microstructures; whereas the additional condition for the m′ to ε_c conversion is that the underlying creep mechanisms are characterized by a

broad distribution in relaxation times (Nowick and Berry, 1982). Since these conditions appear valid for those fibers used to derive the tensile creep model, it follows that equations (8) and (11) can now be combined into a single model for tensile creep and stress relaxation, that is,

$$\varepsilon_c/\varepsilon_e = E A_o \sigma^{n-1} t^p \exp(-B/T) = (1/m') - 1. \quad (12)$$

To verify the empirical model proposed by equation (12), it is assumed in this study that BSR m data for four different types of polycrystalline fibers can be converted by equation (11) to normalized creep strain data. The converted strain data are then used for verification of the equation (12) functional dependencies, determination of the parameters A_o, n, p, and B for the tested fibers, and comparison of model predictions with literature tensile creep results. The equation (11) conversion procedure is used even for fiber types which might be expected to display inequalities between m and m′. As will be shown, however, potential errors in neglecting these inequalities appear small in comparison to temperature-dependent errors.

EXPERIMENTAL

The BSR test was applied to the four types of commercially available polycrystalline ceramic fibers listed in table I. Two fiber types were SiC-based: Nicalon and SCS-6, and two were Al_2O_3-based: PRD-166 and FP. The large diameter SCS-6 fibers were in monofilament form; whereas the small diameter Nicalon, PRD-166, and FP were all in multifilament tow form. Only Nicalon fibers had a sizing which was removed by soaking the tow in acetone for 5 hr. For the nonoxide Nicalon and SCS-6 fibers, BSR tests were performed in an 0.1 MPa argon atmosphere to eliminate oxidation effects. For PRD-166 and FP fibers, BSR tests were performed in air. Average m ratio data were calculated by equation (9) using between 4 and 10 fibers. For an individual BSR test, the standard deviation in the m ratio measurement was less than $\pm$ 0.02 for m values between 0.95 and 0.05.

To examine functional dependencies by the BSR test, the effect of applied strain was measured by subjecting individual fibers to different initial R_o values, e.g., R_o between 0.3 and 2.5 mm for Nicalon, between 15 and 80 mm for SCS-6, and between 5 and 15 mm for the oxide fibers. The effect of time was typically determined by BSR tests of 1, 10, and 100 hr duration. Finally, the effect of temperature was evaluated by BSR tests in the range 900 to 1400 °C. For the majority of time-temperature experiments, PRD and FP fibers were placed in an alumina jig of constant 10 mm radius, i.e., surface strain ~0.1 percent; whereas Nicalon and SCS-6 fibers were tied into loops at a surface strain of either ~0.3 or ~0.5 percent. By this procedure, stress relaxation and normalized creep data were generated at discrete values of applied strain, time, and temperature for each fiber.

RESULTS AND DISCUSSION

Typical BSR m ratio results for the four fiber types are shown in figure 1 as a function of reciprocal temperature. These data were measured for a 1 hr test time at the surface strains indicated in the caption. The creep behavior of all fibers displayed nearly linear stress dependencies, weak time dependencies, but strong exponential temperature dependencies which varied from fiber to fiber. Thus short-time temperature-dependent data such as those in figure 1 provide a simple and convenient method not only for narrowing the test conditions required for the primary creep stage but also for evaluating relative creep resistance of the fibers (Morscher and DiCarlo, 1991). For example, although all commercial fibers tested here began to stress relax near 800 °C, the oxide fibers fully relaxed (m ~ 0) near 1100 °C; whereas the nonoxide SCS-6 and Nicalon fibers did not display full relaxation until ~1400 °C.

The figure 2 log-log plot shows typical normalized creep strain ratio results for the four fibers as a function of applied surface strain ε_o. Test time was 1 hr and test temperatures are indicated in the figure. The fact that the figure 2 data can be best fit with nonhorizontal straight lines indicates that during primary stage creep, a stress power dependence appears valid with n greater than one for all fibers tested here. Best fit n values for the four fiber types are listed in table II. Clearly, the oxide fibers show the greatest deviation from a linear stress dependence; whereas the nonoxide SiC-based fibers display nearly linear behavior in good agreement with available primary stage tensile creep results (DiCarlo, 1986; Tressler and Pysher, 1990).

Regarding time dependence, the log-log plot of figure 3 shows normalized creep strain ratio results for the four fiber types as a function of test time. For the indicated temperatures, test time did not typically exceed 100 hr because normalized creep data could not be accurately measured for strain ratio values greater than 10. That is, due to bend radius measurement errors, the BSR test is most accurate in the primary stage where m ratios from 0.9 to 0.1 yield normalized creep strain ratios from ~0.1 to ~10. Thus any conclusions on model validity must be confined to this range of creep conditions. Nevertheless, within these conditions, data such as those shown in figure 3 do indicate a power law time dependence proposed by the equation (12) creep model. Although the figure 3 results allow direct measurement of the p parameter for each fiber type, a more accurate method described below yields the best fit p values listed in table II. These values which were measured on as-received fibers should be expected to be sensitive to thermal history (DiCarlo, 1986). Also, it should be noted that p values for the oxide fibers differ significantly from the ~1/3 value observed for the SiC-based fibers and for other materials (Andrade, 1910).

For the temperature dependence of fiber creep, the open points of figure 4 show the normalized creep strain results for Nicalon fibers at different test times: 1, 10, and 100 hr. These data were measured at $\varepsilon_o \sim 0.5$ percent so that they could be directly compared in the figure with 1- and 10-hr creep data generated at a tensile stress of 0.5 GPa by Jia et al. (1991). That is, it is assumed that for a fiber with $n > 1$ stress dependence, BSR results at surface strain ε_o can be converted to tensile creep data at an average fiber stress of $\sigma' = E\varepsilon_o/2$ or 0.5 GPa for Nicalon. If the equation (12) creep model is indeed valid, each time data set in figure 4 should be fit by a straight line. In addition, the slope of these lines should be independent of test time and be equal to the empirical parameter B. Furthermore, the BSR data should agree on an absolute scale with the tensile creep data either by interpolation or extrapolation. The dashed lines drawn through each time set in figure 4 show that all these conditions are fulfilled fairly well for the Nicalon fiber, thereby supporting the model and use of the BSR test for creep determination of this fiber.

Although each time data set of figure 4 can be individually used to generate by linear regression a best fit B parameter, it is possible to combine all the data which in turn allows a better measurement of A_o and B plus the additional determination of the Q energy and p parameter for the Nicalon fibers. For example, if Q is constant throughout primary creep, then the abscissa spacing $\Delta(1/T)$ between data sets in figure 4 should be constant and given by the cross-cut method (Damask and Dienes, 1963) as

$$\Delta(1/T) = (R/Q)\ln t_2/t_1. \tag{13}$$

Here t_2/t_1 (=10) is the ratio of test times for adjacent data sets. By using the 1 hr data set as a baseline and shifting the 10 and 100 hr data points to the left by increasing values of $\Delta(1/T)$ and $2\Delta(1/T)$, respectively, one can continuously best fit all the BSR data of figure 4 by linear regression methods until the correlation factor is maximized at a certain $\Delta(1/T)$. At that point, one then has best fit values for parameters A_o and B, plus Q from equation (13) and $p = RB/Q$ from equation (7(b)).

The results of this procedure are shown in figure 5 which also includes the literature tensile data shifted by the optimum $\Delta(1/T)$ value. Best fit values for the Nicalon fiber parameters are listed in table II along with the correlation factor for the B measurement and standard deviation in Q. The high value for the B correlation factor as well as the best fit line in figure 5 again show that the Nicalon fiber not only closely obeys the model assumptions but also that the converted BSR test data is an accurate representation of Nicalon's tensile behavior. It also appears that any bend to tensile conversion error caused by an $n > 1$ stress dependence is lost within the temperature-dependent data scatter.

An alternate but similar approach to the above procedure is to first assume that p is constant so that the 10 and 100 hr data set lines of figure 4 can be shifted downward at constant temperature towards the 1 hr data by a specific amount X given by

$$X = \ln \varepsilon_{c1}/\varepsilon_{c2} = p \ln t_2/t_1. \tag{14}$$

By continuously shifting every 10 and 100 hr data point downward by increasing values of X and 2X, respectively, and using linear regression methods for all BSR data points, one can then determine the optimum X for the maximum correlation factor in the B determination. The result of this procedure yields essentially the same figure 5 best fit line plus the model parameters and correlation factors listed in table II.

Using the temperature shift procedure described above, normalized creep strain data from 1, 10, and 100 hr BSR tests on the other fibers were best fit by linear regression to yield 1 hr straight lines similar to that shown in figure 5 for Nicalon. The results along with available tensile creep data are given in figures 6 to 8 for the SCS-6, PRD-166, and FP fibers, respectively. Best fit A_o, B, p, and Q parameters plus B correlation factors are listed in table II.

Examining the figure 6 results for SCS-6 fibers, one finds very good correlation with model assumptions for all BSR data. However, the tensile data (Morscher et al., 1991), although showing excellent agreement in B, p, and Q, is lower than the converted BSR data by more than a factor of two. This difference, which yields a lower A_o parameter for tension (cf. table II), appears to be related to the composite or nonuniform microstructure of this fiber. That is, the greater creep strain values from the bend test suggest that the outer layers of the SCS-6 fiber are less creep resistant than the inner layers (Morscher et al., 1991).

Regarding the oxide-based fibers, the figure 7 results for PRD show good correlation with model assumptions. Although the single tensile creep point at high temperature (1200 °C) is somewhat greater than extrapolation of the best fit BSR data, this increased creep might be expected due to passage from the primary to the secondary creep stage where additional viscoelastic creep mechanisms can come into play (Raj and Ashby, 1971). Another potential explanation is the thermally-generated loss in effectiveness of ZrO_2 which is added to the Al_2O_3 fiber as a grain pinner to minimize grain sliding and growth (Romine, 1987). Support for the low temperature effectiveness of ZrO_2 can be seen by comparing figure 7 with the figure 8 results for the FP fiber which shows more creep at lower temperatures than PRD. Extrapolation of the best fit FP data, which also shows good correlation with model assumptions, appears to predict lower creep than the single tensile data point. Again, like PRD, this may result from additional viscoelastic creep mechanisms at the higher temperatures.

Although figures 4 to 8 indicate good agreement between the BSR and tensile results, it is recognized that the data are plotted on a log scale which can greatly minimize large differences. For example, the best fit BSR lines may differ from individual BSR and tensile data by less than ±20 percent for the

Nicalon fibers and as much as ±100 percent or greater for the FP fibers. In this study, no attempt has been made to better understand these differences for a variety of reasons. As discussed earlier, tensile creep measurements are difficult and scarce so that reproducibility is an issue. In addition, scatter in creep data is to be expected from many uncontrollable sources including processing and thermally-generated fiber microstructural variations. For the BSR measurements, the assumption that $m = m'$ has inherent errors for nonuniform microstructures or for nonlinear stress dependencies, i.e., $n > 1$. Clearly to understand all of these last effects will require a model fiber with consistent microstructure plus analytical and experimental studies more in-depth than intended here. Notwithstanding these problems, the apparently good agreement found here between tensile creep and BSR data is deemed sufficient evidence to support use of the mechanism-based equation (12) and the table II parameters, not only for gaining insight into the primary stage creep behavior for the four fiber types, but also for generating acceptable predictions of their tensile creep and/or stress relaxation under projected CMC use conditions.

In terms of obtaining basic insight into fiber creep mechanisms, it would appear from the table II parameters that the nonoxide and oxide fibers show distinctly different behavior. That is, in contrast to the Al_2O_3-based fibers, the SiC-based fibers display a nearly linear stress dependence, traditional p values near 1/3, and fairly reproducible creep data. It is generally accepted that if polycrystalline SiC-based materials are to creep at temperatures as low as 1000 °C, the controlling factors are not related to phenomena within the bulk SiC grains, but rather to diffusion mechanisms associated with phases at the grain boundaries. For Nicalon, these phases appear to be related to the presence of processing-induced oxides; whereas for SCS-6, the activation energy, Q, suggests that primary stage creep is controlled by processing-induced silicon or carbon in the grain boundaries (Sargent and Ashby, 1983). For the FP fiber which displays the most extreme values in creep parameters, the activation energy, Q, measured here is close to that for the activation energies measured in polycrystalline alumina for steady state creep caused by grain boundary sliding (Cannon and Langdon, 1983). Beyond these preliminary observations, it is difficult at the present time to definitely ascribe certain phenomena with the table II parameters. It might be conjectured, for example, that the parameters A_o and p are related to grain size whereas the parameter n is controlled by grain boundary thickness. Clearly mechanistic assignments such as these will require future detailed studies involving correlation of microstructural observations with accurate creep measurements.

In terms of using the model for generating creep and/or stress relaxation predictions, it would appear that the table II equation and parameters can be used provided normalized creep strain does not exceed ~10 or the stress relaxation ratio m does not fall below 0.1. For these conditions and a creep-related application, one can then choose specific values for three of the following four variables in order to calculate the fourth: stress, time, temperature, and creep strain. For example, if a certain fiber creep strain limit should not be exceeded for a specific CMC application with a constant service stress of 0.5 GPa and a service time of 100 hr, then the use temperature range for the four fiber types can be estimated using equation (12) and the best fit table II parameters. These temperature estimates are shown in figure 9 for creep strain limits of 0.1 and 1.0 percent. As might be expected from the figure 1 data, the predictions of figure 9 show that the upper use temperature increases with fiber type in the following order: FP, PRD, Nicalon, and SCS-6. It should also be noted that the upper use temperatures for realistic structural conditions are fairly low in comparison to those currently projected for ceramic composites. In addition, the figure 9 upper temperatures vary little with allowed creep strain from 0.1 to 1.0 percent so that absolute inaccuracies in the creep model have only a small effect for this particular calculation. A similar computational procedure can be followed for a stress relaxation application, except now the fourth variable is stress relaxation ratio m instead of creep strain. Although equation (12) can be used for stress relaxation in tension or pure bending, one must be aware that because of the fiber's nonuniform microstructure, the A_o parameter for the SCS-6 fiber in bending is greater than twice that in tension (cf. table II).

Finally, the apparent accuracy of the creep model plus the convenience and simplicity of the BSR test support their general use for estimating the creep-related behavior of other polycrystalline ceramic fibers, especially those for which no tensile creep data currently exist. Using BSR test conditions similar to those described here, one can measure m ratio data which can then be employed to determine the key empirical parameters A_o, n, p, and B. If the m data is strain independent and the fiber is uniform in microstructure, the normalized creep strain data calculated by equation (12) should then accurately represent creep strain in a tensile test for any applied stress. If the m data is strain dependent, one might then assume under tensile loading that $m' = m$ and that $\sigma' = E\varepsilon_o/2$ is an approximate representation of the average applied tensile stress. As demonstrated here, these conversions generate tensile predictions in fairly good absolute agreement with literature data for all fibers except the SCS-6 fiber which has a significantly complex microstructure.

CONCLUSION

In light of the need to understand the high temperature structural behavior of ceramic composites, this study presents a simple approach for modeling the primary stage creep of potential polycrystalline fiber reinforcement. Using a phenomenological model which is based on thermally-activated grain boundary sliding and a simple bend stress relaxation test which is more convenient than the traditional tensile test, this approach has been shown here to yield fairly accurate predictions of primary stage tensile creep strain for a variety of currently available ceramic fibers. The implications of this success are many. For example, for the fibers tested here, one can now predict both creep and stress relaxation behavior for a wide range of stress, strain, time, and temperature conditions. However, due to model and BSR test limitations, these predictions must necessarily be confined to constant stress or strain conditions and to primary stage behavior, that is , creep strain perhaps no more than 10 times the elastic strain. Although restrictive, these limitations still allow some important practical conclusions to be made, such as, relative creep behavior of the different fibers and identification of application conditions where creep-related fiber effects first begin to have serious effects on composite performance. Clearly further studies are needed to determine the full envelope of conditions for model applicability and to implement its predictive capability for variable stress and temperature conditions.

Another important implication of the modeling approach developed here is that it should now allow the materials engineer to decide whether a current polycrystalline ceramic fiber has sufficient creep resistance to be utilized for a specific composite application. If the answer is negative, one might then examine the mechanistic empirical parameters, such as, p and Q, to determine possible microstructural sources for the poor creep resistance. If indeed these sources can be identified, then the fiber producer can judiciously alter the processing conditions of current fibers or alternatively develop new fibers with improved microstructures. As these improved fibers are developed, the simple BSR test can be employed to ascertain progress and then eventually to develop predictive capability for the creep behavior of the final fiber.

REFERENCES

Andrade E.N.: Viscous Flow in Metals. Proc. R. Soc., London, A, vol. 84, June 9, 1910, pp. 1-12.

Cannon, R.W.; and Langdon, T.G.: Review: Creep of Ceramics Part 1 Mechanical Characteristics. J. Mater. Sci., vol. 18, 1983, pp. 1-50.

Damask, A.C.; and Dienes, G.J.: Point Defects in Metals. Gordon and Breach, Science Publishers Inc., NY, 1963.

DiCarlo J.A.: Creep of Chemically Vapour Deposited SiC Fibers. J. Mater. Sci., vol. 2, 1986, pp. 217-224.

DiCarlo, J.A.: High Temperature Structural Fibers - Status and Needs. NASA TM-105174, 1991.

Feltham P.: On the Representation of Rheological Results with Special Reference to Creep and Relax ation. Br. J. Appl. Phys., vol. 6, no. 1, 1955, pp. 26-31.

Jia, N.; Bodet, R.; and Tressler, R.E.: Creep and Creep Rupture Behavior of Si-C-O and Si-N-C-O Based Continuous Fibers. Presented at the 93rd Annual Meeting of the American Ceramic Society, Cincinnati, OH, 1991.

Ke, T.S.: Experimental Evidence of the Viscous Behavior of Grain Boundary in Metals. Phys. Rev., vol. 71, 1947, pp. 533-546.

Ke, T.S.; and Zener, C.: Structure of Cold-Worked Metals as Deduced from Anelastic Measurements. Symposium on the Plastic Deformation of Crystalline Solids, Proc., pp. 185-192.

Morscher, G.N.; and DiCarlo, J.A.: A Simple Test for Thermomechanical Evaluation of Ceramic Fibers. J. Am. Ceram. Soc., vol. 75, no. 1, 1992, pp. 136-140.

Morscher, G.N.; DiCarlo, J.A.; and Wagner, T.: Fiber Creep Evaluation by Stress Relaxation Measurements. Ceram. Eng. Proc., vol. 12, no. 7-8, 1991, pp. 1032-1038.

Nowick, A.S.; and Berry, B.S.: Anelastic Relaxation in Crystalline Solids. Academic Press, 1982.

Raj, R.; and Ashby, M.F.: On Grain Boundary Sliding and Diffusional Creep. Metall. Trans., vol. 2, 1971, pp. 1113-1127.

Romine, J.C.: New High-Temperature Ceramic Fiber. Ceram. Eng. Sci. Proc., vol. 8, 1987, pp. 755-765.

Sargent, P.M.; and Ashby, M.F.: Deformation-Mechanism Maps for Silicon Carbide. Scripta Metall., vol. 17, 1983, pp. 951-957.

Tressler, R. E.; and Pysher, D. J.: Mechanical Behavior of High Strength Ceramic Fibers at High Temperatures. Satellite Symposium 4 on high temperature super conductors, The 7th International Meeting on Modern Ceramic technologies, Triste, Italy, P. Vincerzini, eds., Elsevier, 1991.

TABLE I. - FIBER SPECIMENS AND PROPERTIES

Type	Processing	Diameter, μm	Primary phases
Nicalon*	Polymer pyrolysis	12-16	β-SiC; SiO_2; C
SCS-6**	Chemical vapor deposition	142	β-SiC
PRD-166***	Slurry spinning	20	α-Al_2O_3; ZrO_2
FP***	Slurry spinning	20	α-Al_2O_3

* Nippon Crabon Co., Tokyo, Japan.
** Textron Specialty Materials, Lowell, Massachusettes.
*** DuPont de Nemours & Co. Inc., Wilmington, Delaware.

TABLE II. - BEST FIT PARAMETERS FOR CREEP (ε_c) AND STRESS RELAXATION (m)

$$\varepsilon_c = (\sigma/E)\,[(1/m) - 1] = A_o\,\sigma^n t^p \exp(-B/T)$$

	E^a, GPa	$A_o{}^b$	n	p^c	B, K	Correlation factor[d]	Q^e, kJ/mol
Nicalon	200	2.2×10^5	1.2	0.40	24 200	0.980	[e]500±65
SCS-6 (BSR)	400	2.8×10^5	1.1	0.37	25 800	0.991	580±38
SCS-6 (Tensile)	400	1.0×10^5	[f]1.1	.37	[f]25 800		
PRD 166	370	7.0×10^{10}	1.35	0.53	41 000	0.964	640±70
FP	370	49×10^{10}	1.5	0.58	41 150	0.959	590±76

[a]Fiber modulus (approximate).
[b]Parameter A_o applies for stress (σ) in GPa, time (t) in hr, and temperature (T) in Kelvin.
[c]Time parameter p calculated from $p = RB/Q$.
[d]Correlation factor for linear regression to determine B parameter.
[e]Controlling creep energy Q and standard deviation.
[f]Assumed from bend results.

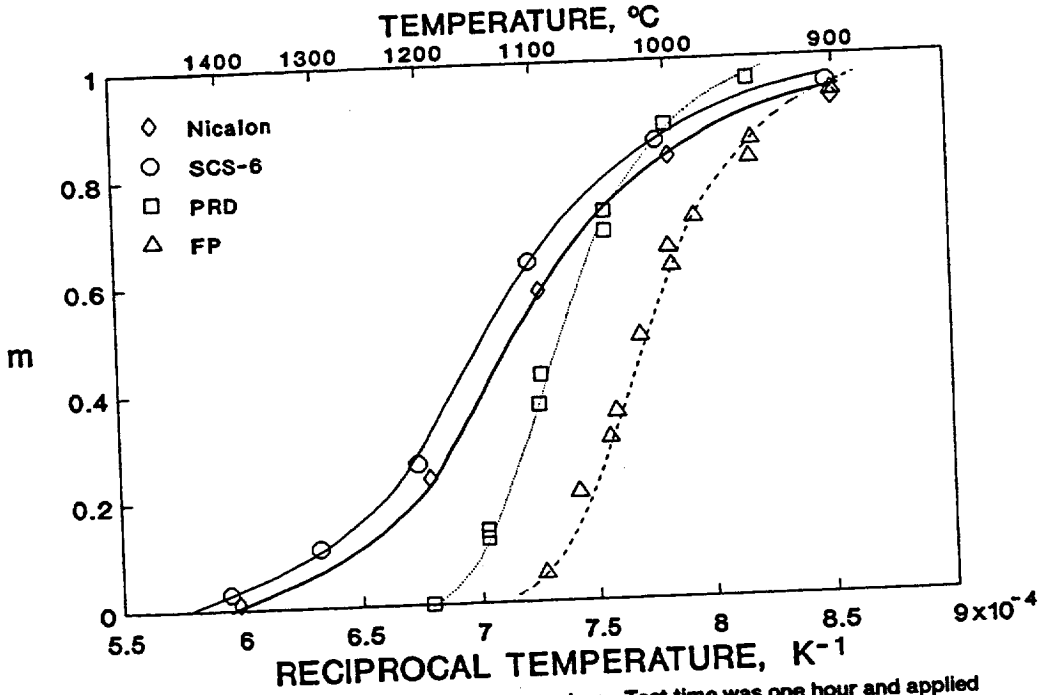

Figure 1.—BSR m ratio versus reciprocal temperature. Test time was one hour and applied surface strains were ~ 0.3 percent and ~ 0.1 percent for the nonoxide and oxide fibers, respectively.

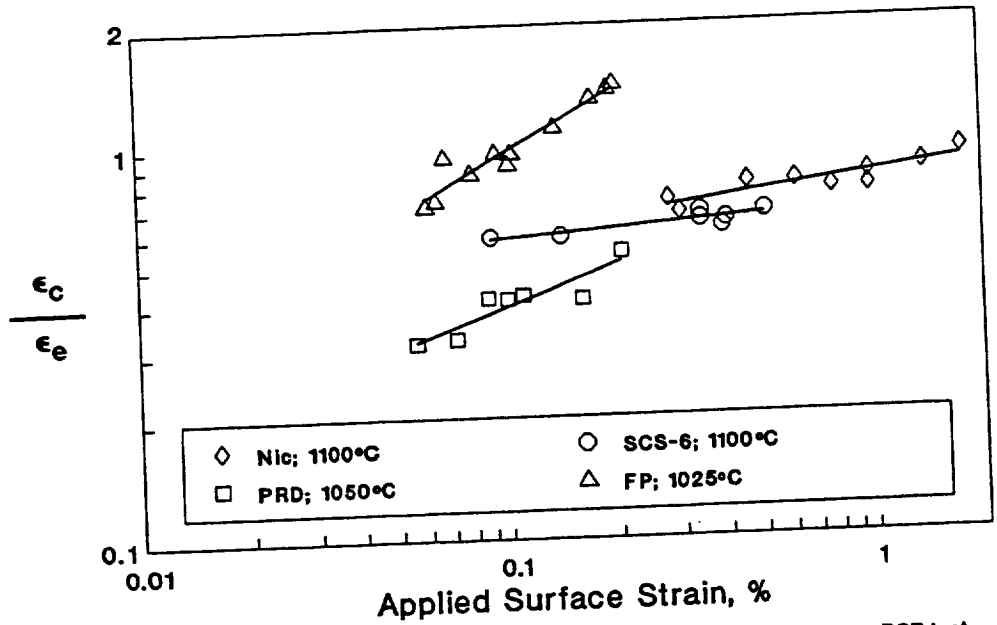

Figure 2.—Normalized creep strain versus applied surface strain for one-hour BSR test.

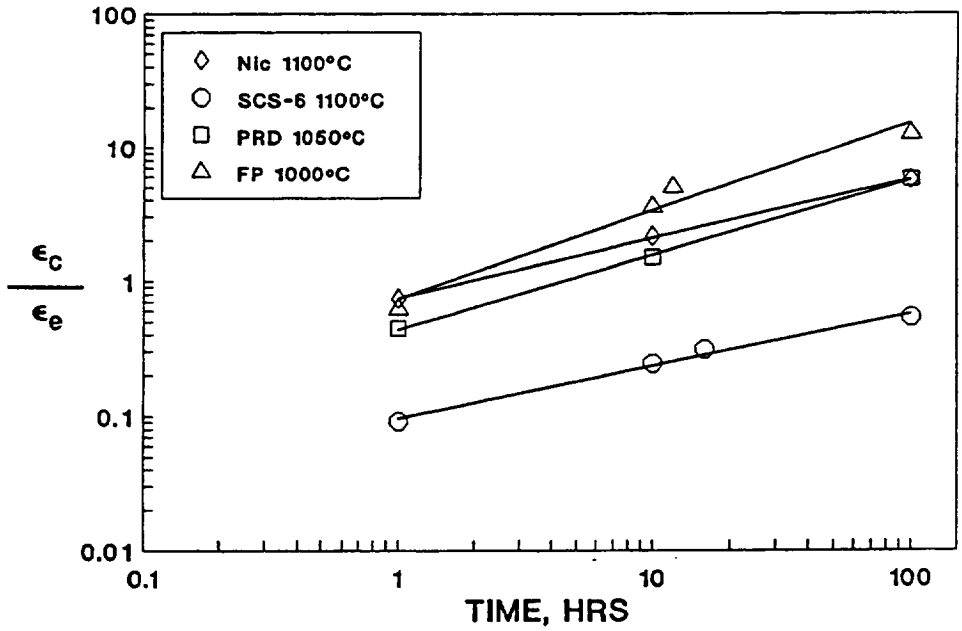

Figure 3.—Normalized creep strain versus BSR test time. Applied surface strains were ~ 0.3 percent and ~ 0.1 percent for the nonoxide and oxide fibers, respectively.

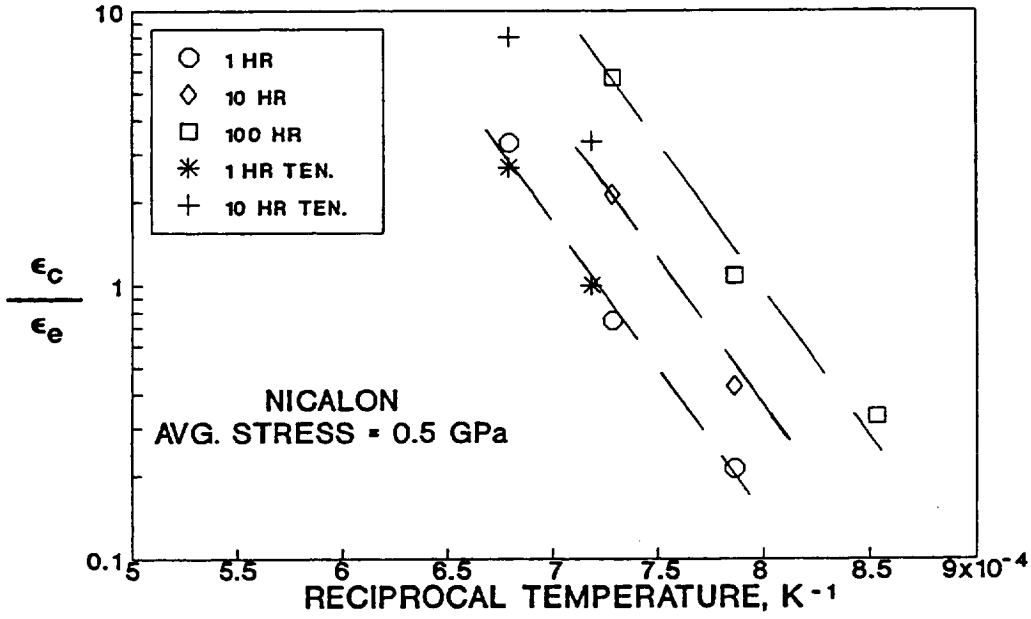

Figure 4.—Normalized creep strain versus reciprocal temperature for Nicalon fibers. Tensile data from Jia et al. (1991).

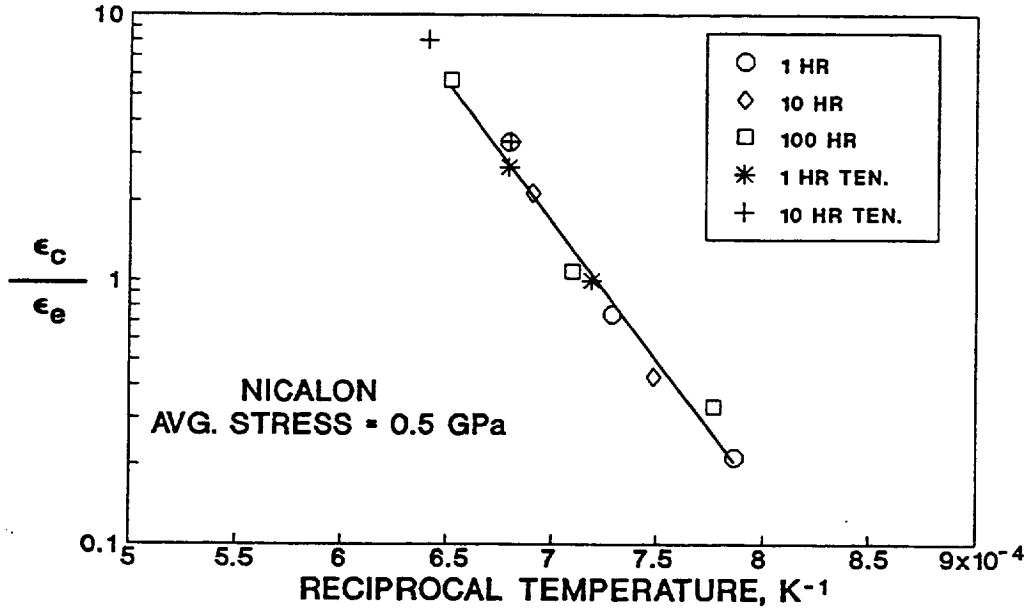

Figure 5.—Normalized creep strain versus reciprocal temperature for Nicalon fiber. Data at 10 and 100 hours were shifted in temperature to yield best fit one-hour line. Tensile data from Jia et al. (1991).

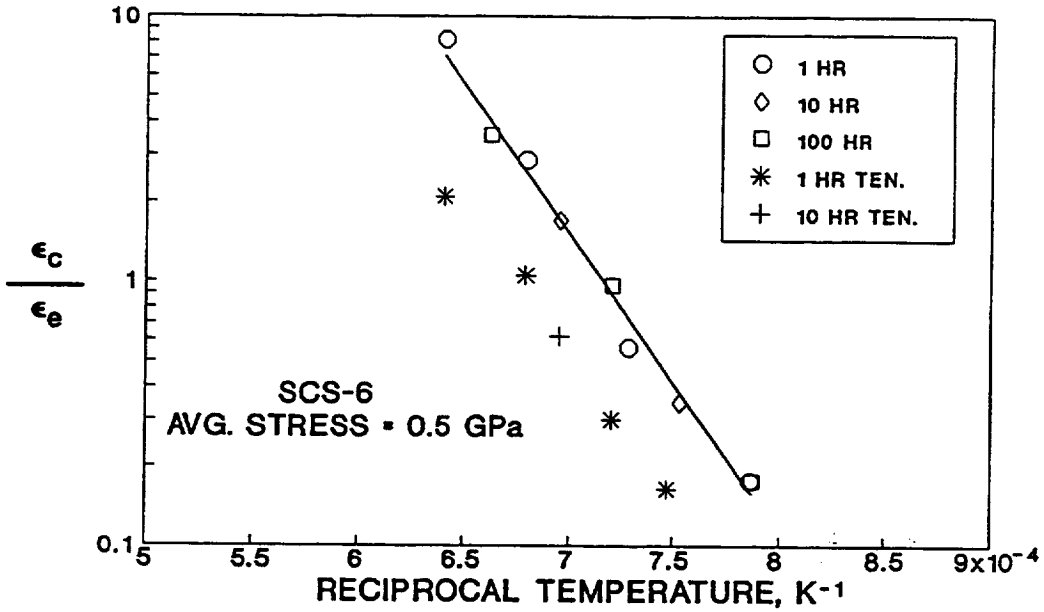

Figure 6.—Normalized creep strain versus reciprocal temperature for SCS-6 fiber. Data at 10 and 100 hours were shifted in temperature to yield best fit one-hour line. Tensile data from Morscher at et al. (1991).

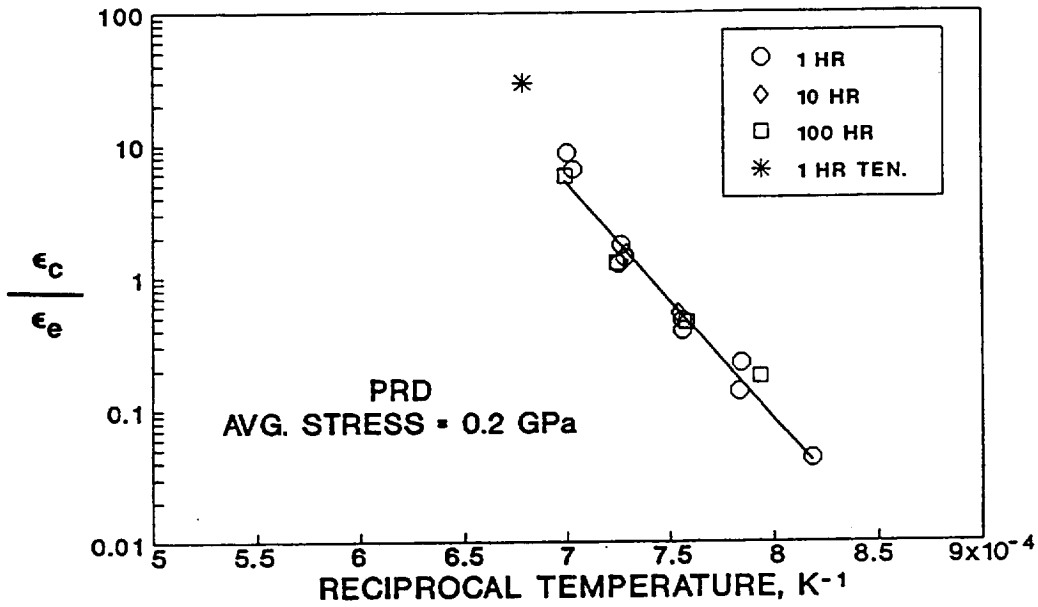

Figure 7.—Normalized creep strain versus reciprocal temperature for PRD fiber. Data at 10 and 100 hours were shifted in temperature to yield best fit one-hour line. Tensile creep was performed at 0.15 GPa (Tressler and Pysher, 1990).

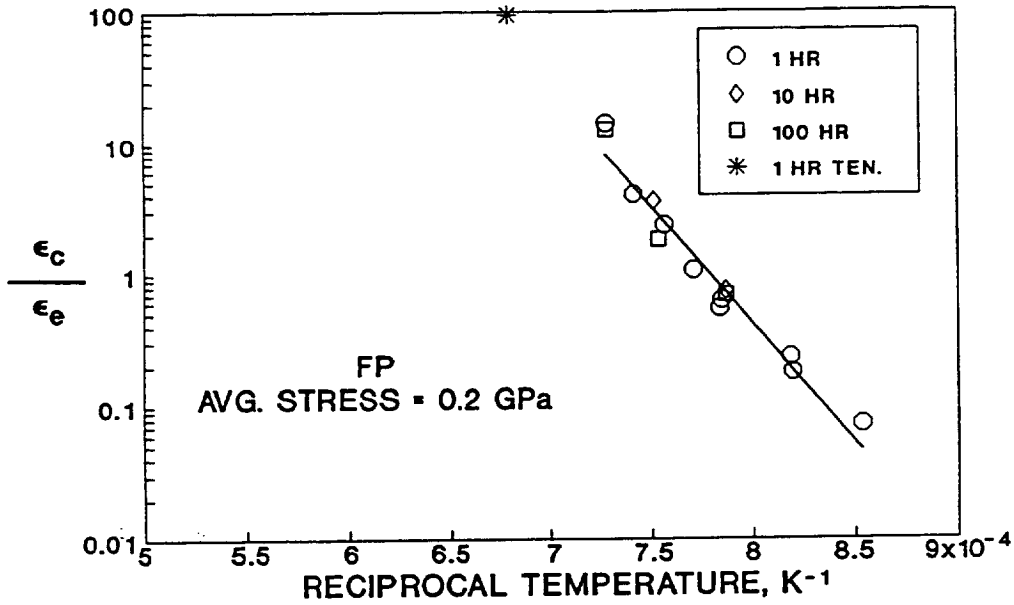

Figure 8.—Normalized creep strain versus reciprocal temperature for FP fiber. Data at 10 and 100 hours were shifted in temperature to yield best fit one-hour line. Tensile creep was performed at 0.1 GPa (Tressler and Pysher, 1991).

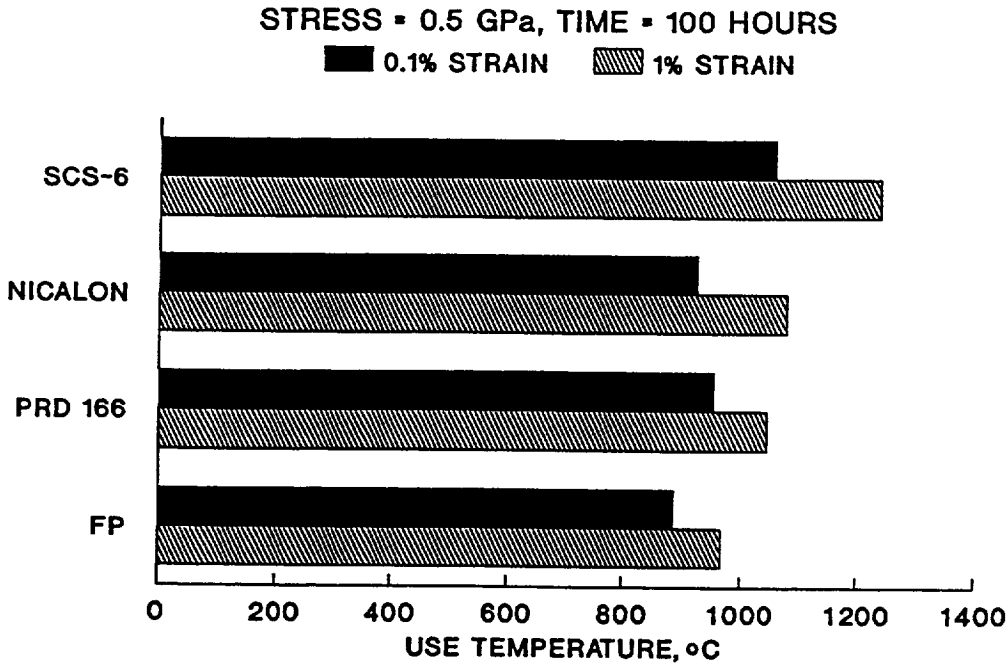

Figure 9.—Estimate of use temperature ranges for four fiber types based on the indicated application conditions and the model parameters of Table II.

REPORT DOCUMENTATION PAGE

Form Approved
OMB No. 0704-0188

1. AGENCY USE ONLY (*Leave blank*)	2. REPORT DATE	3. REPORT TYPE AND DATES COVERED
	August 1994	Technical Memorandum

4. TITLE AND SUBTITLE

Creep and Stress Relaxation Modeling of Polycrystalline Ceramic Fibers

5. FUNDING NUMBERS

WU-510-01-50

6. AUTHOR(S)

James A. DiCarlo and Gregory N. Morscher

7. PERFORMING ORGANIZATION NAME(S) AND ADDRESS(ES)

National Aeronautics and Space Administration
Lewis Research Center
Cleveland, Ohio 44135-3191

8. PERFORMING ORGANIZATION REPORT NUMBER

E-6785

9. SPONSORING/MONITORING AGENCY NAME(S) AND ADDRESS(ES)

National Aeronautics and Space Administration
Washington, D.C. 20546-0001

10. SPONSORING/MONITORING AGENCY REPORT NUMBER

NASA TM-105394

11. SUPPLEMENTARY NOTES

Prepared for the 1991 Winter Annual Meeting sponsored by the American Society of Mechanical Engineers, Atlanta, Georgia, December 1-6, 1991. James A. DiCarlo, NASA Lewis Research Center and Gregory N. Morscher, Case Western Reserve University, Cleveland, Ohio 44106 and NASA Resident Research Associate at Lewis Research Center (work funded by NASA Grant NAG3-1141). Responsible person, James A. DiCarlo, (216) 433-5514.

12a. DISTRIBUTION/AVAILABILITY STATEMENT

Unclassified - Unlimited
Subject Category 24

12b. DISTRIBUTION CODE

13. ABSTRACT ***(Maximum 200 words)***

A variety of high performance polycrystalline ceramic fibers are currently being considered as reinforcement for high temperature ceramic matrix composites. However, under mechanical loading about 800 °C, these fibers display creep-related instabilities which can result in detrimental changes in composite dimensions, strength, and internal stress distributions. As a first step toward understanding these effects, this study examines the validity of a mechanism-based empirical model which describes primary stage tensile creep and stress relaxation of polycrystalline ceramic fibers as independent functions of time, temperature, and applied stress or strain. To verify these functional dependencies, a simple bend test is used to measure stress relaxation for four types of commercial ceramic fibers for which direct tensile creep data are available. These fibers include both nonoxide (SCS-6, Nicalon) and oxide (PRD-166, FP) compositions. The results of the bend stress relaxation (BSR) test not only confirm the stress, time, and temperature dependencies predicted by the model, but also allow measurement of model empirical parameters for the four fiber types. In addition, comparison of model tensile creep predictions based on the BSR test results with the literature data show good agreement, supporting both the predictive capability of the model and the use of the BSR text as a simple method for parameter determination for other fibers.

14. SUBJECT TERMS

Creep; Stress relaxation; Fibers; Polycrystalline; Silicon carbide; Alumina; Modeling; Primary stage; Transient creep

15. NUMBER OF PAGES

20

16. PRICE CODE

A03

17. SECURITY CLASSIFICATION OF REPORT	18. SECURITY CLASSIFICATION OF THIS PAGE	19. SECURITY CLASSIFICATION OF ABSTRACT	20. LIMITATION OF ABSTRACT
Unclassified	Unclassified	Unclassified	